THE JOURNAL OF PHYSICAL CHEMISTRY C

Article

pubs.acs.org/JPCC

# Depth Profiling Photoelectron-Spectroscopic Study of an Organic Spin Valve with a Plasma-Modified Pentacene Spacer

Jhen-Yong Hong,[†] Yin-Ming Chang,[†] Cheng-Hao Chuang,[†] Kai-Shin Li,[†] You-Cih Jhang,[†] Hung-Wei Shiu,[‡] Chia-Hao Chen,[‡] Wen-Chung Chiang,*[,§] and Minn-Tsong Lin*[,†,∥]

[†]Department of Physics, National Taiwan University, 10617 Taipei, Taiwan

[‡]National Synchrotron Radiation Research Center, 30076 Hsinchu, Taiwan

[§]Department of Physics, Chinese Culture University, 11114 Taipei, Taiwan

[∥]Institute of Atomic and Molecular Sciences, Academia Sinica, 10617 Taipei, Taiwan

**ABSTRACT:** We report an enhanced magnetoresistance (MR) in an organic spin valve with an oxygen plasma-treated pentacene (PC) spacer. The spin valve containing PC without the treatment shows no MR effect, whereas those with moderately plasma-treated PC exhibit MR ratios up to 1.64% at room temperature. X-ray photoelectron spectroscopy with depth profiling is utilized to characterize the interfacial electronic properties of the plasma-treated PC spacer which shows the formation of a derivative oxide layer. The results suggest an alternative approach to improve the interface quality and in turn to enhance the MR performance in organic spin valves.

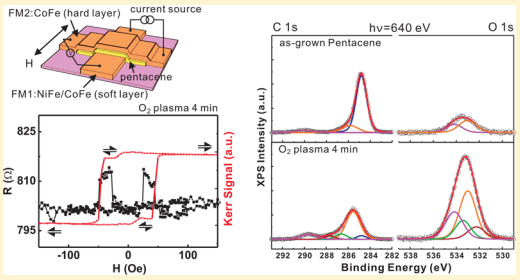


## INTRODUCTION

Organic semiconductors (OSC), owing to their ease of processing, mechanical flexibility, and highly tunable chemical properties, are promising candidates for low-cost electronic and spintronic device applications.[1] Recently, a large magnetoresistive (MR) effect with exceptionally long spin diffusion length has been demonstrated in organic spin valves (OSVs) comprising $La_{0.67}Sr_{0.33}MnO_3$ (LSMO)/OSC/ferromagnet (FM) trilayered structure.[2,3] However, in these LSMO-based OSVs, the MR effect diminishes quickly as temperature rises and hardly sustains the desirable working temperature (i.e., room temperature) because the spin polarization of LSMO is highly temperature-dependent.[4,5] To achieve room-temperature OSV operation, electrode materials other than LSMO need to be involved. The trials include the revisit of conventional 3d transition FM metals such as Co and Fe,[6,7] but the conductivity mismatch between the electrode and OSC would deplete the spin injection from FM into OSC.[7,8] Nevertheless, effective spin injection can be restored by inserting a thin insulating tunnel barrier such as $Al_2O_3$ between the FM electrode and the OSC spacer.[5,9−11] As an alternative approach in this study, OSVs with a pentacene (PC) spacer have been prepared, and the derivative oxide at the FM/OSC interface created by plasma-induced modification on the PC surface took the place of the aforementioned $Al_2O_3$ barrier.

Pentacene (PC) is a model organic semiconductor material which has widely been used as the active layer in organic thin film transistors (OTFTs).[12,13] The high mobility (≥1 $cm^2/V{\cdot}s$) and excellent crystalline quality of PC make it an ideal medium for charge carrier transport.[12,13] Nevertheless, when used in layered structures such as OSV, pentacene poses a potential problem because metals deposited onto pentacene may either penetrate the surface or diffuse into pentacene that degrades the device performance. In fact, metal diffusion has been attributed as the primary cause of pinholes and defects in the organic layer in OSVs.[3,5,14] The insertion of a buffer layer at the organic/metallic interface[9,15,16] or the modification of the organic layer with functionalized surfaces[17] has been reported to prevent the metal penetration or diffusion and in turn to improve the device performance. Organic surface modification by oxygen plasma has also been demonstrated for adhesion improvement, while the desirable bulk properties of the organic material are maintained.[18,19] The technique of plasma treatment is a versatile tool for surface chemical modification in many applications such as carbon nanotube electronics,[20] organic biosensors,[21] and surface adhesion improvement of organics.[18] Being a dry, low-temperature, and time-efficient process, the advantages of plasma treatment also include the confinement of its modification solely on the surface of a material. In this paper, we demonstrate that the PC-based OSVs with oxygen-plasma treatment exhibit room-temperature spin-dependent transport. We further investigate the "in-depth" electronic profile of the plasma-treated PC and confirm the establishment of a thin derivative oxide layer. The results suggest that the combination of PC and a plasma-induced surface oxide is helpful to aid the MR performance in OSVs.

## EXPERIMENTAL SECTION

As schematically illustrated in Figure 1(a), the organic spin valve is constructed in the sequence of NiFe (22 nm)/CoFe

**Received:** March 20, 2012
**Revised:** September 17, 2012
**Published:** September 18, 2012





dx.doi.org/10.1021/jp3026557 | J. Phys. Chem. C 2012, 116, 21157−21161

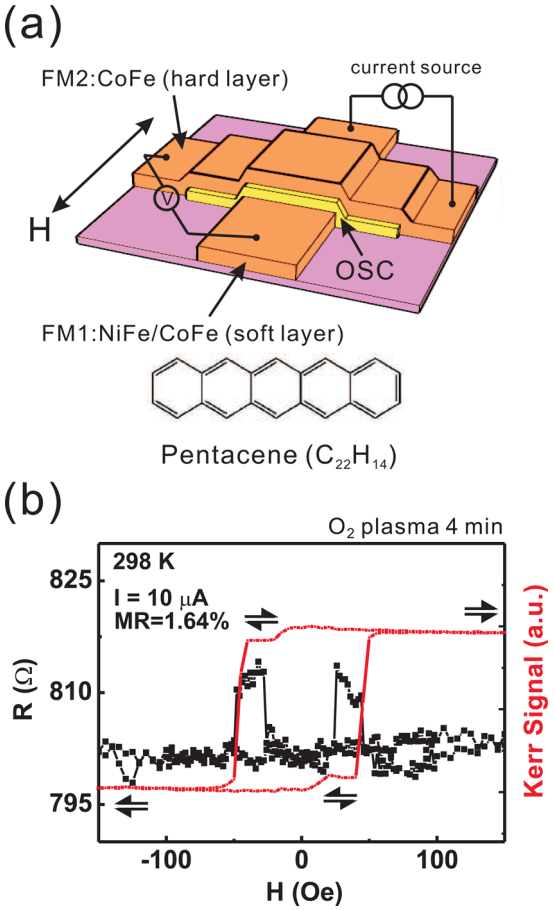


**Figure 1.** (a) Schematic diagram of the trilayered organic spin valve (OSV). The organic semiconductor (OSC) spacer is made of pentacene, whose molecular structure is indicated below. (b) The room-temperature magnetoresistive (black, referenced to the left vertical axis) and the MOKE hysteresis (red, referenced to the right vertical axis) curves of an OSV with 20.5 nm PC treated by oxygen plasma for 4 min. Both measurements were made at room temperature.

(15 nm)/PC (20.5 nm)/CoFe (30 nm) with the OSC PC spacer sandwiched between two crossed ferromagnetic electrodes, in which the combination of NiFe/CoFe acts as the soft FM layer whereas the capping CoFe acts as the hard layer.[22,23] The PC layer was prepared by thermal evaporation followed by oxygen-plasma treatment (at the power of 100 W and the pressure of 30 mTorr) of various exposure times, whereas the NiFe and the CoFe layers were made by dc sputtering at an Ar working pressure of 5 mTorr. The Current-Perpendicular-to-the-Plane (CPP) resistance and the Magneto-Optical Kerr Effect (MOKE) measurements were employed to characterize the magnetoresistive (MR) effect and the magnetization configuration of the two FM electrodes. The electronic properties of PC with different exposure time to oxygen plasma were investigated separately on bilayered samples (made without the capping CoFe electrode but under conditions identical to the OSV samples) using X-ray photoelectron spectroscopy (XPS) at Beamline 09A1 of the National Synchrotron Radiation Research Center (NSRRC) in Taiwan. The 0.12 eV XPS energy resolution was set by the pass energy of 5.85 eV in the Hemispherical Sector Analyzer (HSA). To estimate the thickness of the derivative PC oxide created by the plasma treatment, the depth profile of the plasma-treated PC layer was performed using an in-house X-ray source excited XPS (VG ESCA Scientific Theta Probe (2000)) equipped with an Ar etching source.

## RESULTS AND DISCUSSION

The cycling of junction resistance with field of a PC-based spin valve (with 20.5 nm thick PC treated by oxygen plasma for 4 min) is indicated by the black curve in Figure 1(b). The curve displays the typical pseudospin-valve-type characteristics at room temperature with a MR ratio of 1.64%. Here, the MR ratio is defined as $\Delta R/R_P = (R_{AP} - R_P)/R_P$, where $R_P$ and $R_{AP}$ are the resistances when the magnetizations of the FM electrodes are in parallel and antiparallel configurations, respectively. The red curve in Figure 1(b) gives the hysteresis loop obtained by the MOKE measurement, in which a typical two-step pseudospin-valve behavior is also observed. The change of MR follows closely the switching of the relative magnetization orientation of the two electrodes, as indicated in Figure 1(b).

Figure 2 shows the junction resistances and the MR ratios of a series of OSVs whose 20.5 nm thick PC spacers have been

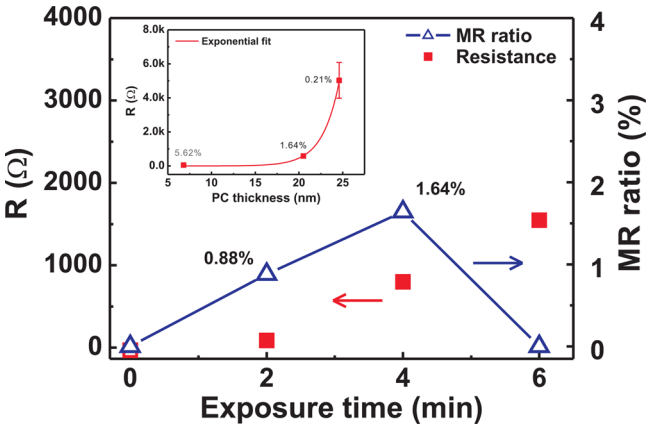


**Figure 2.** Variations of junction resistance (red squares, referenced to the left axis) and MR ratio (blue open triangles, referenced to the right axis) with oxygen-plasma exposure time for OSVs with a 20.5 nm PC spacer. The negative resistance of the 0 min sample (indicated by the open square) is due to a current distribution effect, and the solid blue lines linking the MR data are a guide to the eye. The inset shows the variation of junction resistance versus PC thickness for samples whose PC spacers have been treated by plasma for 4 min. The numbers by the data points indicate the MR ratios.

treated by oxygen plasma for various exposure times. The sample containing the as-grown PC spacer without the treatment exhibits a negative measured resistance and no MR effect. The negative value of resistance is due to the inhomogeneity of current distribution when the resistance of the junction itself is much smaller than the resistance of the electrodes.[24] The low junction resistance of the as-grown sample suggests that the existence of pinholes and defects in the PC layer possibly resulted from the subsequent sputtering process of the top CoFe layer and the diffusion of the electrode material into PC. The sample with PC treated by 2 min oxygen plasma shows a positive junction resistance of 88 Ω and a MR ratio of 0.88%, signaling the occurrence of spin-polarized transport. When the plasma exposure time is raised to 4 min, the junction resistance increases to 800 Ω, while the MR ratio reaches 1.64%. This junction resistance is twice the resistance of


dx.doi.org/10.1021/jp3026557 | J. Phys. Chem. C 2012, 116, 21157–21161

the electrodes (≅400 Ω). At 6 min exposure time, the junction resistance continues to rise, but the MR ratio drops to zero. Previous studies have shown that the transport of charge carriers is very sensitive to the morphology of the semiconductor surface and the electronic defects at the semiconductor−insulator interface.[25] The 6 min plasma exposure time might have overly oxidized the PC layer, creating undesirable defects and nonspin-conserving scatterings that devastate the MR effect. A quick review of Figure 2 suggests that the ≈4 min plasma exposure time sets an opportune window to create an effective derivative oxide layer over the PC surface for the junction. Samples with different PC thicknesses and treated by 4 min oxygen plasma also reveal a MR effect of different magnitudes. The sample with 6.8 nm thick PC exhibits a MR effect of 5.62%, but this high MR ratio is more likely (or at least partially) due to the current distribution effect in a junction with low junction resistance.[24,26] The sample with 24.6 nm thick PC shows a MR effect of 0.21% (note that the MR ratio for the sample with 20.5 nm thick PC is 1.64%). The decrease of MR with increasing spacer thickness is known as the consequence of spin-memory loss effect in spin-related transport.[10,27]

Because of the relatively low junction resistances of our samples (keep in mind that there's an energy barrier of ≈1 eV for PC grown on Co to make charge transport difficult[28]), whether the charge transport is actually occurring through the PC layer or simply by direct tunneling through the oxide channel or defects in some local thin areas needs to be clarified. The inset of Figure 2 plots the junction resistance versus PC thickness for a series of OSVs whose PC spacers have been treated by oxygen plasma for 4 min. Under the circumstance of fixed plasma exposure time and hence fixed oxide layer thickness, which is about 1.8 nm as estimated by the depth profiling of XPS (see below), the junction resistance scales exponentially with the PC thickness. This exponential scaling behavior has been reported in previous OSV works and has been used to classify effective transport in organics.[9,11] The result shown in the inset of Figure 2 suggests that in our OSV samples the electric transport is more likely occurring and dominated via the PC layer rather than through the oxide channel or defects.

Figures 3(a), 3(b), and 3(c) show, respectively, the C 1s and O 1s core-level XPS spectra for 0 min (as-grown), 2 min, and 4 min oxygen plasma-treated PC. In Figure 3(a), the main peak (C1) in the C 1s spectrum at binding energy (BE) 284.8 eV represents the $sp^2$-formed carbon in the PC structure,[29] whereas the peaks at BE 285.6 eV (C2) and BE 289.9 eV (C5) are attributed to the C−O chemical bond and the O−C═O bond attached to PC, respectively.[30] The appearance of C2 and C5 could result from the surface oxidation when the PC layer was exposed to the ambience. Figures 3(b) and 3(c) show that when the PC layers are treated by oxygen plasma the oxygen-related bonds in the C 1s state appear at the higher BE side, including peak C2 at BE 285.6 eV for the C−O bond, peak C3 at BE 286.6 eV for C−O−C, peak C4 at BE 287.6 eV for C═O, and peak C5 at BE 289.6 eV for O−C═O.[30] Compared with the C 1s state of the as-grown PC, the number of oxidation peaks increases upon treatment, evidencing the effect of chemical modification by oxygen plasma. In contrast, the $sp^2$-formed C═C state diminishes upon the treatment due to the reconstruction of oxidation bonds. As for the O 1s state, the as-grown PC shows a broad peak with two oxygen components: peak O1 at BE 533.0 eV for the C−O bond and

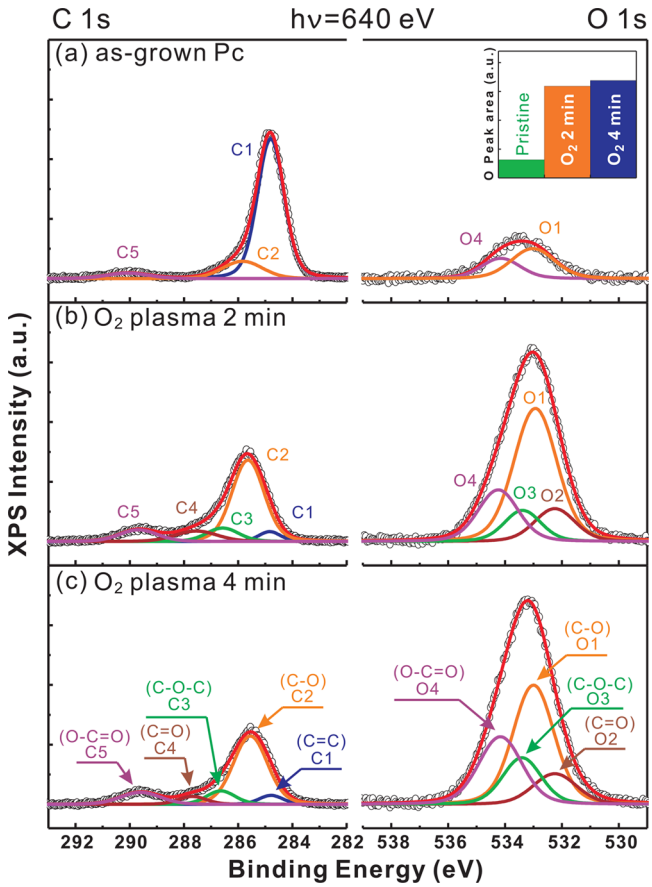


**Figure 3.** XPS C 1s and O 1s spectra of bilayered PC (20.5 nm)/CoFe (30 nm) samples with (a) as-grown PC, (b) PC treated by oxygen plasma for 2 min, and (c) PC treated by oxygen plasma for 4 min. The open circles and the red curves represent the original XPS data and the sum of the fitted components, respectively. The inset column shows the integrated intensities of the O 1s spectra for the three samples.

peak O2 at BE 534.2 eV for O−C═O (see Figure 3(a)). The spectra of 2-min and 4-min plasma-treated PC, as seen in Figures 3(b) and 3(c), show an enhanced peak of the O 1s state which can be resolved into four components, namely, peak O1 at BE 533.0 eV for the C−O bond, peak O2 at BE 532.2 eV for C═O, peak O3 at BE 533.4 eV for C−O−C, and peak O4 at BE 534.2 eV for O−C═O.[30] The plasma treatment also increases the number of components of the oxygen−carbon group during the formation of PC oxide, which is consistent with the C 1s profile. The inset column of Figure 3 compares the intensities integrated over the O 1s spectra for the three samples considered. The intensities of the treated samples are substantially larger than that of the as-grown sample. The slight difference between the intensities of the two treated samples could be due to the discrepancy of the probing depth, as the photoemission electrons are highly surface sensitive.

The depth profiles of the C 1s, O 1s, and Fe $2p_{3/2}$ states are performed on a bilayered sample consisting of 20.5 nm of PC treated by 4-min oxygen plasma and 30 nm of CoFe, by a series of etching processes (using Ar plasma) to remove a thin surface layer with each removal followed by an immediate XPS scan. The variations of the maximum peak intensity with etching depth for the C 1s, O 1s, and Fe $2p_{3/2}$ signals are indicated by black, red, and green symbols in Figure 4(a), respectively. From 0 to ∼1.8 nm in the depth profile, the intensity of the C 1s signal slowly increases, while that of the O 1s rapidly decreases


dx.doi.org/10.1021/jp3026557 | J. Phys. Chem. C 2012, 116, 21157−21161

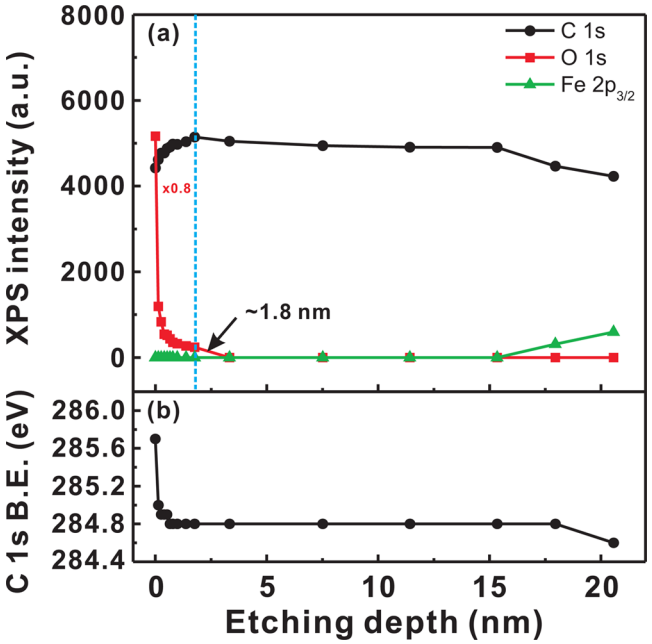


**Figure 4.** (a) Maximum XPS peak intensity for C 1s, O 1s, and Fe $2p_{3/2}$ states and (b) the C 1s binding energy profile, both as functions of etching depth, as recorded on a bilayered PC (20.5 nm)/CoFe (30 nm) sample with PC treated by oxygen plasma for 4 min.

and approaches zero. As the etching process goes further, the signal intensity of C 1s remains unchanged, whereas those of O 1s and Fe $2p_{3/2}$ are almost negligible until reaching a threshold at ~16 nm when the Fe $2p_{3/2}$ signal starts to pick up and the C 1s signal goes down. The profile gives a clear indication that the oxidation depth of the 4-min plasma-treated PC is approximately 1.8 nm. Underneath the surface oxide lies the pristine PC, and the final intensity changes indicate the approaching of the PC/CoFe interface.

Figure 4(b) shows the position (in terms of binding energy) of the maximum XPS C 1s peak as a function of depth. The peak position starts at 285.7 eV before etching, which is attributed to the C−O bond that belongs to the surface oxidation group resulting from the oxygen-plasma treatment. As Ar ions lift off the topmost layer of the oxidized PC, the position of the C 1s peak moves quickly toward 284.8 eV, which is attributed to the C−C bond within the PC structure. The peak position remains flat until 18 nm in depth. From 18 to 20.5 nm, the C 1s peak position shifts from 284.8 to 284.6 eV, accompanied by the increase of the Fe $2p_{3/2}$ signal (see Figure 4(a)), indicating that the etching process is reaching the end of PC. Combining the results of Figure 4(a) and Figure 4(b), we estimate the thickness of the derivative oxide created by the 4-min oxygen-plasma treatment around 1.8 nm, with the majority of the original PC remaining intact. Thus, the treatment of oxygen plasma is proven effective in modifying the surface layer of PC without affecting its bulk electronic properties, suggesting an alternative approach to engineer the OSC/FM interface and to improve the MR performance in OSV devices.

## CONCLUSION

In conclusion, our study of organic spin valves with a moderately plasma-modified PC spacer shows a magnetoresistive effect with MR ratio up to 1.64% at room temperature. The C 1s and O 1s core-level XPS spectra recorded on the oxygen plasma-treated PC indicate the formation of a derivative oxide layer on the PC surface. The XPS depth profile recorded on the 4-min oxygen plasma-treated sample reveals the actual thickness of the derivative oxide and further demonstrates that oxygen plasma acts only on the surface of the PC without affecting its bulk electronic properties of the majority part. These results suggest that the use of a thin derivative oxide layer created upon the organic layer by plasma treatment could be an effective approach to improve the MR performance in OSV devices.

## AUTHOR INFORMATION

### Corresponding Author

*E-mail: wchiang@faculty.pccu.edu.tw; mtlin@phys.ntu.edu.tw.

### Notes

The authors declare no competing financial interest.

## ACKNOWLEDGMENTS

This work was supported in part by the National Science Council of Taiwan under Grant No. NSC 99-2120-M-002-005 and No. NSC 99-2112-M-034-001.

## REFERENCES

(1) Naber, W. J. M.; Faez, S.; van der Wiel, W. G. *J. Phys. D: Appl. Phys.* **2007**, *40*, R205−R228.
(2) Dediu, V.; Murgia, M.; Matacotta, F.; Taliani, C.; Barbanera, S. *Solid State Commun.* **2002**, *122*, 181−184.
(3) Xiong, Z. H.; Wu, D.; Valy Vardeny, Z.; Shi, J. *Nature* **2004**, *427*, 821−824.
(4) Wang, F. J.; Yang, C. G.; Vardeny, Z. V.; Li, X. G. *Phys. Rev. B* **2007**, *75*, 245324.
(5) Dediu, V.; Hueso, L. E.; Bergenti, I.; Riminucci, A.; Borgatti, F.; Graziosi, P.; Newby, C.; Casoli, F.; De Jong, M. P.; Taliani, C.; et al. *Phys. Rev. B* **2008**, *78*, 115203.
(6) Wang, F.; Xiong, Z.; Wu, D.; Shi, J.; Vardeny, Z. *Synth. Met.* **2005**, *155*, 172−175.
(7) Jiang, J. S.; Pearson, J. E.; Bader, S. D. *Phys. Rev. B* **2008**, *77*, 035303.
(8) Schmidt, G.; Ferrand, D.; Molenkamp, L. W.; Filip, A. T.; van Wees, B. J. *Phys. Rev. B* **2000**, *62*, R4790−R4793.
(9) Santos, T. S.; Lee, J. S.; Migdal, P.; Lekshmi, I. C.; Satpati, B.; Moodera, J. S. *Phys. Rev. Lett.* **2007**, *98*, 016601.
(10) Shim, J. H.; Raman, K. V.; Park, Y. J.; Santos, T. S.; Miao, G. X.; Satpati, B.; Moodera, J. S. *Phys. Rev. Lett.* **2008**, *100*, 226603.
(11) Li, K.-S.; Chang, Y.-M.; Agilan, S.; Hong, J.-Y.; Tai, J.-C.; Chiang, W.-C.; Fukutani, K.; Dowben, P. A.; Lin, M.-T. *Phys. Rev. B* **2011**, *83*, 172404.
(12) Lin, Y.-Y.; Gundlach, D.; Nelson, S.; Jackson, T. *IEEE Electron Device Lett.* **1997**, *18*, 606−608.
(13) Shtein, M.; Mapel, J.; Benziger, J. B.; Forrest, S. R. *Appl. Phys. Lett.* **2002**, *81*, 268−270.
(14) Vinzelberg, H.; Schumann, J.; Elefant, D.; Gangineni, R. B.; Thomas, J.; Buchner, B. *J. Appl. Phys.* **2008**, *103*, 093720.
(15) Di, C.-A.; Liu, Y.; Yu, G.; Zhu, D. *Acc. Chem. Res.* **2009**, *42*, 1573−1583.
(16) Chu, C.-W.; Li, S.-H.; Chen, C.-W.; Shrotriya, V.; Yang, Y. *Appl. Phys. Lett.* **2005**, *87*, 193508.
(17) Maisch, S.; Buckel, F.; Effenberger, F. *J. Am. Chem. Soc.* **2005**, *127*, 17315−17322.
(18) Egitto, F. D.; Matienzo, L. J. *IBM J. Res. Dev.* **1994**, *38*, 423−439.
(19) Cho, S.-J.; Choi, J.-W.; Bae, I.-S.; Nguyen, T.; Boo, J.-H. *Jpn. J. Appl. Phys.* **2011**, *50*, 01AK02.
(20) Hou, Z.; Cai, B.; Liu, H.; Xu, D. *Carbon* **2008**, *46*, 405−413.
(21) Xue, C.-Y. C.; Yang, K.-L. K. *Langmuir* **2007**, *23*, 5831−5835.

(22) Chang, Y.-M.; Li, K.-S.; Chiang, W.-C.; Lin, J.-Y.; Lin, M.-T. *Phys. Rev. B* **2009**, *79*, 012401.
(23) Chang, Y.-M.; Li, K.-S.; Huang, H.; Tung, M.-J.; Tong, S.-Y.; Lin, M.-T. *J. Appl. Phys.* **2010**, *107*, 093904.
(24) Lenczowski, S. K. J.; van de Veerdonk, R. J. M.; Gijs, M. A. M.; Giesbers, J. B.; Janssen, H. H. J. M. *J. Appl. Phys.* **1994**, *75*, 5154−5159.
(25) Gershenson, M. E.; Podzorov, V.; Morpurgo, A. F. *Rev. Mod. Phys.* **2006**, *78*, 973−989.
(26) Van de Veerdonk, R.; Nowak, J.; Meservey, R.; Moodera, J.; De Jonge, W. *Appl. Phys. Lett.* **1997**, *71*, 2839−2841.
(27) Parkin, S. *Annu. Rev. Mater. Sci.* **1995**, *25*, 357−388.
(28) Tiba, M. V.; de Jonge, W. J. M.; Koopmans, B.; Jonkman, H. T. *J. Appl. Phys.* **2006**, *100*, 093707.
(29) Baldacchini, C.; Allegretti, F.; Gunnella, R.; Betti, M. G. *Surf. Sci.* **2007**, *601*, 2603−2606.
(30) Beamson, G.; Briggs, D. *High Resolution XPS of Organic Polymers*; JOHNWILEY & SONS: Chichester (UK), 1992.